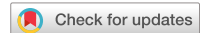


# scientific data

**OPEN**  
**DATA DESCRIPTOR**



## Soil erosion susceptibility maps and raster dataset for the hydrological basins of North Africa

Adil Salhi<sup>1</sup>✉, Sara Benabdouahab<sup>2</sup> & Essam Heggy<sup>3,4</sup>

Soil erosion in North Africa modulates agricultural and urban developments as well as the impacts of flash floods. Existing investigations and associated datasets are mainly performed in localized urban areas, often representing a limited part of a watershed. The above compromises the implementation of mitigation measures for this vast area under accentuating extremes and continuous hydroclimatic fluctuations. To address this deficiency, we use the Revised Universal Soil Loss Equation to map surface erosion, providing the first insight into the decadal impacts of land degradation, which are largely unconstrained on North Africa's continental scale. We generate soil erosion maps for the major hydrological basins of North Africa using Google Earth Engine and multiple hydroclimatic and land use datasets, covering 5.8 million square kilometers. The generated geospatial dataset integrates land use, soil erodibility, slope, vegetation cover, and land practices. The resulting product is an expansive and publicly available Soil erosion susceptibility maps and rasters dataset (SESMAR). This dataset is a crucial step toward understanding the drivers of soil erosion in this vast, poorly characterized area as well as its potential to be used for future soil conservation campaigns for both agricultural and urban planning. We validate SESMAR using the Global Rainfall Erosivity Database (GloREDa) and the European Soil Data Centre (ESDAC) datasets as well as published peer-reviewed reports across 20 watersheds, demonstrating a robust agreement in assessing the average annual soil loss values and soil erosion classes in local areas covered by independent study teams. Our continental maps show commendable accuracy, supporting scientists, practitioners, and policymakers in their efforts for more resilient land management practices across North Africa to mitigate rising hydroclimatic extremes.

### Background & Summary

Soil erosion in North Africa modulates agricultural and urban developments as well as the turbidity of flows arising from flash floods and, hence, their destructive power. Physical investigations and associated datasets often focus on localized urban areas, typically in the outflow of a watershed overlooking the upstream characteristics. This has resulted in several damages to urban structures and loss of human lives associated with the increase in extreme events and coastal storminess (Normand and Heggy<sup>1</sup>). Furthermore, there is no unified dataset that can compare the physical characteristics of soil erosion of the main watersheds in North Africa which results in a limited understanding of the role of land degradation in modulating the impacts of hydroclimatic extremes. This deficiency hampers effective assessment of hydroclimatic risks, agricultural developments, policymaking, and targeted mitigation of erosion impacts. Moreover, the region grapples with additional complexities stemming from large-scale hydroclimatic shifts, which exacerbate soil erosion rates and pose significant environmental threats<sup>2,3</sup>. The absence of reliable large-scale maps compromises the sustainability and resilience of this vast area under rising extreme events and continuous climatic fluctuations.

High-resolution soil erosion maps and datasets are critical for supporting sustainable land management and mitigating the impacts of hydroclimatic hazards<sup>4</sup>. The importance of comprehensive datasets to understand soil erosion patterns on a larger scale cannot be overstated. Additional complexities stemming from large-scale

<sup>1</sup>Geography and Development group, Abdelmalek Essaadi University, FLSH, Martil, Morocco. <sup>2</sup>Economic and Environmental Geology and Hydrology group, University of Barcelona, Barcelona, Spain. <sup>3</sup>University of Southern California, Viterbi School of Engineering, 3737 Watt Way, Powell Hall of Engineering, Los Angeles, CA, 90089, USA.

<sup>4</sup>NASA Jet Propulsion Laboratory, California Institute of Technology, 4800 Oak Grove Drive, Pasadena, CA, 91109, USA. ✉e-mail: [asalhi@uae.ac.ma](mailto:asalhi@uae.ac.ma)

hydroclimatic shifts exacerbate soil erosion rates and pose significant environmental threats<sup>5</sup>. The absence of reliable large-scale maps compromises the sustainability and resilience of vast areas under rising extreme events and continuous climatic fluctuations<sup>6</sup>.

As a result of these limitations in mitigating soil erosion across densely urbanized areas of North Africa, outflow migrations towards the northern shores of the Mediterranean basin are increasingly observed in part due to the rising impacts of hydroclimatic fluctuations combined with inefficient mitigation strategies<sup>7,8</sup>. These migration patterns, in which the population would abandon agricultural and urban areas, further aggravate the footprint of soil erosion. This emphasizes the urgent need for sustainable land management practices based on accurate datasets to address and alleviate the strains induced by population displacement<sup>9</sup>. Moreover, the readiness to tackle these impacts associated with large-scale soil erosion is compounded by persistent instabilities across multiple locations in North Africa<sup>10</sup>. Political unrest, socio-economic disparities, and environmental vulnerabilities intertwine to create a complex landscape where the consequences of soil erosion are magnified. Consequently, addressing these challenges necessitates a multifaceted approach based on physical geospatial products and datasets that can support environmental conservation efforts to provide data-driven decision-making.

To address the above limitations in soil erosion data availability, this investigation generates comprehensive continental maps and datasets of soil erosion, providing a first insight into the impacts of land degradation across North Africa. Based on the Revised Universal Soil Loss Equation (RUSLE) model<sup>11</sup>, we use Google Earth Engine code over 5.8 million square kilometers (19% of Africa's total land area), encompassing five southern Mediterranean countries of the continent, i.e., Morocco, Algeria, Tunisia, Libya, and Egypt, with a total population above 210 million inhabitants.

Unlike localized studies at the city scale, our dataset covers the entire hydrological basins of North Africa, creating a spatial coverage comparable to other existing global datasets<sup>4</sup>, which operate at different geographic and temporal resolutions. In contrast, our dataset enables finer and localized insights into soil erosion patterns. Indeed, global-scale assessment, while invaluable for understanding broad trends, may not capture the specific environmental variations and localized factors influencing soil erosion in the watersheds of North Africa. Our dataset addresses this gap by integrating high-resolution hydroclimatic and land use data tailored to the region's unique geophysical conditions. This regional focus is essential for effective soil conservation and land management practices, offering detailed, actionable insights that global datasets might overlook. Moreover, our dataset's validation using peer-reviewed reports across 20 watersheds demonstrates its accuracy and applicability for regional soil conservation efforts. This validation process, which compares our data products with the physical outcomes of published studies using similar methodologies, ensures the reliability of our process in assessing average annual soil loss and erosion classes in local areas.

The analysis of land use reflects the diversity of the regional characteristics (Fig. 1a). Agricultural activities dominate the Delta and the banks of the Nile, the Moroccan Atlantic plains, and the Mediterranean coastal plains from Tangier (Morocco) to Sfax (Tunisia). Limited coastal areas in Tripoli and Benghazi (Libya) also feature agricultural land use. The Rif and Atlas Mountains belts are primarily covered by forests and grasslands, serving as essential habitats for biodiversity. Along the coasts, major urban centers and built-up areas are concentrated, with cities like Cairo (Egypt), Marrakech, and Fes (Morocco) standing out as notable interior urban hubs. In contrast, large parts of North Africa are characterized by shrublands, the expansive Sahara Desert, and vast stretches of bare ground, reflecting arid and sparsely populated areas.

The soil texture exhibits considerable variability across North Africa (Fig. 1b). Coarser-textured sandy soils dominate the desert regions, particularly in the Sahara, where fine soils such as clay are less prevalent due to wind erosion and limited vegetation cover. In contrast, finer-textured soils like loam, clay loam, and silty clay loam are found along the coastal plains, especially in agricultural zones such as the Nile Delta and parts of the Moroccan and Tunisian Mediterranean coastlines. These finer soils contribute to higher water retention capacities, which is critical for agricultural productivity in these regions. The presence of clay-rich soils in the northern areas indicates past alluvial processes and sediment deposition, further influencing land use suitability and vegetation patterns.

Elevations datasets show distinct patterns and features, characterized by topographical variations and divergent gradients (Fig. 1c). In the western part, the high mountain belts of the Atlas Mountains and the Rif Mountains act as natural barriers, separating the narrow Mediterranean plains from the relatively larger Atlantic plains. These mountain ranges contribute to rugged terrains and significant elevation variations. Moving toward the central and southern areas, the landscape is dominated by the desertic highlands of the Hoggar mountain range, characterized by vast arid terrains. In contrast, the eastern part consists of more extensive plains, except for the Eastern Desert belt and the Sinai Desert in Egypt. Steep slopes are primarily associated with the mountain belts, making them prominently present in the western part and along the Mediterranean coast of Morocco, Algeria, and Tunisia (Fig. 1d).

North Africa has witnessed several geological processes and tectonic events in the Pleistocene and Holocene, resulting in a varied and complex geological setting (Fig. 1e). The presence of multiple terrains ranging in age from Archean to Quaternary contributes to the geological complexity<sup>12</sup>. Three major tectonostratigraphic domains can be identified: the Precambrian province, the Variscan (Paleozoic) fold belt, and the Atlas-Alpine (Mesozoic-Cenozoic) system<sup>13</sup>. The northern coastline, stretching from Morocco to Egypt, is characterized by folded and faulted sedimentary rocks, with the Atlas Mountains acting as a prominent feature influencing the geology, lithology, climatology, and soil properties of the surrounding areas<sup>3,13</sup>. The Sahara Desert is known for its extensive aeolian landforms, including sand dunes, sand sheets, and gravel plains. Prevailing wind patterns and local topography influence these landforms. Beneath the Sahara Desert lies the Saharan Platform, which encompasses the central and eastern parts of the investigated area, including various sedimentary basins such as the Taoudeni Basin and the Murzuk Basin<sup>14–16</sup>.

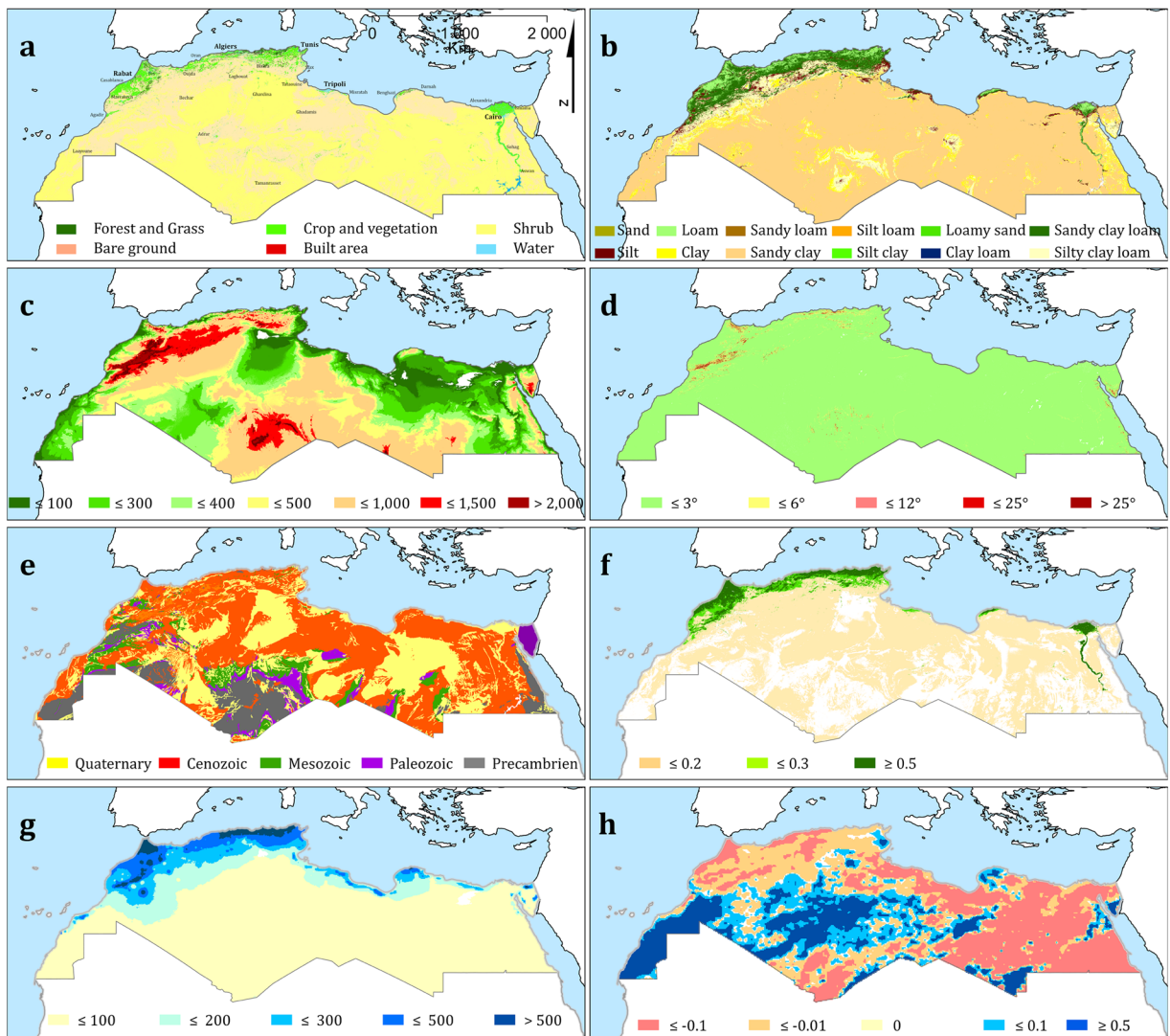


**Fig. 1** Main physical and hydroclimatic characteristics of North Africa (a). Land use/land cover in 2022 (Sentinel), (b) Soil texture at 0 cm depth (OpenLandMap Soil Texture Class)<sup>40</sup>, (c) Digital elevation model obtained from Shuttle Radar Topography Mission (in meters), (d) slope (in degree), (e) Simplified classification of lithological units by age<sup>12</sup>, (f) The average Normalized Difference Vegetation Index (MODIS/MCD43A4\_006\_NDVI) in 2022 (without unit), (g) The average annual precipitation during the last 43 years (1981–2023) (calculated from the Climate Hazards Group InfraRed Precipitation with Station data (CHIRPS) rainfall dataset), (h) The precipitation cumulative annual anomaly during the last 24 years (2000–2023) compared to the reference period (1950–1999) (calculated from the ERA5-Land Monthly Aggregated dataset).

The Normalized Difference Vegetation Index (NDVI) correlates well with the observed land use patterns (Fig. 1f), indicating variations in vegetation density and distribution. Areas with intensive agricultural activities, such as the Nile Delta and banks, the Moroccan Atlantic plains, and the Mediterranean coastal plains between Tangier and Sfax, exhibit high NDVI values. These areas display vibrant and dense vegetation cover due to irrigation practices and/or favorable climatic conditions for crop growth. The Rif and Atlas Mountains belts, known for their forests and grasslands, also show relatively high NDVI values, indicating healthier vegetation due to better precipitation and cooler temperatures. On the other hand, areas dominated by shrubs, the Sahara Desert, and bare ground generally have low NDVI values, indicating limited photosynthetic activity and sparse vegetation cover.

The significance of photosynthetic activity in specific areas of North Africa is linked to the abundance of precipitation (Fig. 1g). The 42-year (1981–2023) average of annual precipitation (calculated from the Climate Hazards Group InfraRed Precipitation with Station data (CHIRPS) rainfall dataset) shows the most substantial downpours in the Atlas Mountains belt and the northern coastal regions, including Tripoli and Benghazi. The Atlas belt acts as a conduit, directing moisture-laden masses toward the northern areas of North Africa, resulting in drier conditions in the southern and eastern parts of the region<sup>3</sup>. Consequently, the Atlas Mountain belt and the surrounding northern areas exhibit increased greenness and vegetation growth due to the availability

Soil Texture	K-factor
Sand	0.05
Loamy Sand	0.07
Sandy Loam	0.23
Silt	0.35
Loam	0.25
Sandy Clayey Loam	0.18
Silty Loam	0.30
Clay	0.20
Silty Clay	0.19
Sandy Clay	0.09
Clayey Loam	0.22
Silty Clayey Loam	0.28

**Table 1.** K-factor value according to soil texture<sup>38</sup>.

of moisture. In the case of the Nile Delta, its remarkable greenness is attributed to two significant contributors: the Nile River and groundwater resources in Egypt which play crucial roles in sustaining high levels of photosynthetic activity<sup>17–19</sup>.

Furthermore, anomalies in precipitation are observed in the wettest areas over the past 23 years (2001–2023). North Africa has experienced a precipitation deficit of more than 10%, leading to drier conditions (Fig. 1h). This reduction in rainfall poses significant concerns for the ecological balance and agricultural productivity in these regions. Decreased precipitation levels result in water stress, decreased crop yields, and potential ecological impacts on wildlife habitats and overall ecosystem resilience<sup>20,21</sup>.

## Methods

The Revised Universal Soil Loss Equation (RUSLE) is used to assess soil erosion. It was developed by the USDA Natural Resources Conservation Service (NRCS) based on five factors: rainfall erosivity (R), soil erodibility (K), slope length and gradient (LS), cover and management (C), and support practices (P)<sup>11</sup>. It calculates the average annual soil loss (A) (t/ha/year) according to Eq. 1<sup>11</sup>. Different datasets were rescaled to a spatial resolution of 500 meters to obtain data for each factor.

$$A = R \cdot K \cdot LS \cdot C \cdot P \quad (1)$$

The five factors R, K, LS, C, and P are calculated for each year of the investigation period (2001–2023). Afterward, they are crossed according to Eq. 1 to generate an annual soil erosion image for each corresponding year. Subsequently, the mean factorial maps and the mean soil erosion map for the entire investigation period are computed by averaging the annual images. Finally, the resulting mean images were mapped, and the pixel-based factorial values and annual soil loss values (in t/ha/y) were calculated.

The rainfall erosivity (R-factor) is the susceptibility of precipitation and runoff to cause erosion, potentially uprooting small soil particles. It depends on the dynamic energy of precipitation, its frequency, and its duration. Traditionally, the R-factor is calculated using detailed rainfall intensity data, including storm energy and maximum 30-minute intensity (I30)<sup>11</sup>. However, such high-resolution temporal data may not be consistently available across all regions, especially in data-scarce environments like North Africa. To address this limitation, we employ a widely used alternative approach based on the annual precipitation (P) and the maximum precipitation in 24 hours of the considered year ( $P_i$ )<sup>22</sup>, which are more commonly available from the CHIRPS Daily dataset (Eq. 2). Despite the data resolution challenges, our analysis remains robust and reliable as detailed in data validation section below. Notably, this modified equation has been validated and applied in similar research contexts where high-frequency rainfall data is scarce<sup>23–29</sup>. CHIRPS Daily dataset are processed to obtain the precipitation values for each year.

$$R = 143 \cdot \log(P \cdot P_i^2 \cdot 10^{-6}) + 89.7 \quad (2)$$

For the K-Factor, soil texture data is retrieved from the Open Land Map Soil Texture dataset. Given the absence of a comprehensive dataset with the required spatial and temporal resolution covering all of North Africa, soil types are assigned specific K-factor values based on generalized estimates derived from published literature<sup>30</sup> (Table 1). These estimates provide a basis to approximate regional variations in soil erodibility within the twelve identified soil texture classes.

For LS-Factor, Digital Elevation Model (DEM) data from the NASA SRTM (Shuttle Radar Topography Mission) dataset are utilized. Slope values are derived and converted to percentages. The LS factor was computed using an adapted equation tailored to our study's spatial and data resolution requirements<sup>27–29</sup>. Specifically, we utilize Eq. 3 (where L is the slope length and S is the percent slope). This equation integrates empirical coefficients adjusted to reflect regional land and topographic characteristics, enhancing the accuracy of erosion risk assessments. Variations in LS factor equations, including adjustments in coefficients are discussed in soil erosion

modeling literature<sup>31,32</sup>, reflecting the need to tailor erosion models to specific environmental conditions and data availabilities.

$$LS = \frac{\sqrt{L}}{100} \cdot (0.76 + 0.53 \cdot S + 0.076 \cdot S^2) \quad (3)$$

For C-Factor, the Normalized Difference Vegetation Index (NDVI) data from the MODIS/MCD43A4\_006\_NDVI dataset are used based on Eq. 4<sup>33,34</sup> (where  $\alpha$  and  $\beta$  are dimensionless parameters that, according to several studies, have been determined to be  $\alpha=2$  and  $\beta=1$  for achieving optimal results<sup>35,36</sup>).

$$C = e^{\left(-\alpha \cdot \frac{NDVI}{\beta - NDVI}\right)} \quad (4)$$

For the P-factor, the land cover data from the MCD12Q1.006 MODIS Land Cover Type Yearly Global dataset were employed. The Annual International Geosphere-Biosphere Program (IGBP) classification band (LC\_Type1) is used to assign P-factor values<sup>37</sup> to each land use/land cover class of the corresponding year at the pixel scale.

Our investigation utilizes a Google Earth Engine (GEE) code to assess soil erosion in all the basins of continental North Africa over the period from January 1, 2001, to December 31, 2023. The code loads a basin dataset from the hydro-basin dataset (WWF/HydroSHEDS/v1/Basins/hybas) and filters it to obtain a specific basin (Area of Interest) identified by the HYBAS\_ID. The latter is a mapping product that provides hydrographic information for regional and global-scale applications at various scales<sup>38</sup>. The basins range from level 1 (coarse) to level 12 (detailed), using HYBAS\_ID codes. Hence, considering the diverse range of basin sizes in North Africa, we strategically utilize various hierarchical levels to precisely identify and characterize the desired basin. It is crucial to acknowledge that, in this context, several basins incorporate sub-basins, thereby introducing a level of intricacy to the delineation process. For the convenience of prospective users, it's noteworthy that the resultant raster datasets cover extensive basins, which can be further partitioned into smaller or medium-sized sub-basins as necessary.

After meticulously iterating through the code across North African basins, a distinct pattern emerged. Basins within the Sahara Desert exhibited predominantly low to very low erosion susceptibility, indicating minimal spatial variation. On the contrary, basins in the northern mountainous ranges, whether partially or entirely located there, demonstrate significant erosion rates and spatial disparities. These variations are closely tied to factors such as precipitation abundance, steep terrain, and friable lithology. Consequently, the focus was directed toward creating soil erosion susceptibility maps and corresponding rasters specifically for the northern mountainous range basins. For a detailed overview, refer to Table 2, which provides HYBAS\_ID and descriptive information.

For each selected basin, the code begins by creating a list of years within the specified temporal range and subsequently initiates the creation of an Image-Collection dedicated to annual soil erosion images (Fig. 2). This iterative process traverses each year within the defined time range. The Revised Universal Soil Loss Equation (RUSLE) calculation involves several steps. The computation of the R-Factor involves leveraging precipitation data from the CHIRPS dataset<sup>39</sup>. For the K-Factor, the Soil Erodibility factor is derived based on soil type data obtained from the 'Open Land Map Soil Texture Class (USDA System)' dataset<sup>40</sup>. In the LS-Factor Calculation step, the code encompasses the computation of the Length-Slope factor using the SRTM dataset<sup>41</sup>. Determining the C-Factor involves utilizing NDVI data available in the MOD13A2.061 Terra Vegetation Indices dataset<sup>42</sup>. The P-Factor is calculated as part of the Support Practice factor, combining land cover and slope information. The land cover is retrieved from the MCD12Q1.006 MODIS Land Cover Type Yearly Global<sup>43</sup> and the slope information is computed based on the SRTM<sup>41</sup>. The final step, RUSLE Calculation, involves multiplying the calculated factors (R, K, LS, C, P) to obtain an annual soil erosion image<sup>11</sup>.

Subsequently, the code computes the average annual soil loss over the entire period and clips the result to the area of interest. The code further computes average soil loss statistics for each class of soil erosion. To facilitate the visualization of soil loss patterns, an image with pixel areas is created, including an additional band for the soil loss classification. This image is then reduced to calculate the sum of pixel areas for each soil loss class. The subsequent retrieval of group information contains class numbers and corresponding areas. The code efficiently extracts these details, converting the areas to square kilometers. It is noteworthy that all datasets underwent rescaling to a uniform spatial resolution of 500 meters. This harmonization ensures consistency and comparability across the diverse datasets utilized in the analysis.

## Data Records

The resulting extensive maps and dataset are publicly available in a scientific open-access repository (<https://doi.org/10.5281/zenodo.1047896>), offering the first continental soil erosion susceptibility maps and associated raster data products<sup>44</sup>.

The soil erosion susceptibility maps and raster dataset for all the continental basins of North Africa are entitled SESMAR. This dataset offers maps and readily classified TIFF raster images that enhance usability for researchers and practitioners alike (see example in Fig. 3). The dataset is divided into 22 compressed-format rasters, each with a single band, which characterizes soil loss susceptibility across distinct classes. These classes, ranging from 'Very low' to 'Very High' provide nuanced insights into annual soil loss rates per hectare.

The comprehensive classification system embedded in the SESMAR dataset facilitates a detailed understanding of soil loss susceptibility across various geographical locations. This resource can be employed for environmental and agricultural planning, aiding stakeholders in identifying and prioritizing areas for targeted soil

Basin*	Main cities	Basin HYBAS_ID	HydroSHEDS level	Basin area (km <sup>2</sup> )
Tarfaya	Tarfaya, Morocco El Ouatia, Morocco	1050030450	5	44,493
Draa	Ouarzazate, Morocco Zagoura, Morocco	1040028960	4	95,887
Souss-Tensift	Marrakech, Morocco Agadir, Morocco	1040028970	4	74,062
Oum Er Rabie	Beni Mellal, Morocco Khenifra, Morocco	1040029430	4	38,047
Casablanca	Casablanca, Morocco Rabat, Morocco	1040029440	4	20,099
Sebou	Fes, Morocco Kenitra, Morocco	1040029700	4	37,812
Loukkos	Tangier, Morocco Larache, Morocco	1040029710	4	7,415
Mediterranean Morocco	Tetouan, Morocco Nador, Morocco	1050029810	5	12,942
Moulouya	Berkane, Morocco Guercif, Morocco	1040028970	4	54,237
Oujda	Oujda, Morocco Oran, Algeria	1050030230	5	30,253
Mecheria	Tendrara, Morocco Mecheria, Algeria	1040040740	4	48,908
Bouarfa	Bouarfa, Morocco Bechar, Algeria	1040040300	4	120,044
Ghardaia	Ghardaia, Algeria Hassi Fehal, Algeria	1040040740	4	146,406
Chlef	Chlef, Algeria Tiaret, Algeria	1050030460	5	44,493
North Mediterranean	Algiers, Algeria Bizerte, Tunisia	1050030460	5	66,781
Jendouba	Jendouba, Tunisia Tebessa, Algeria	1050031290	5	23,171
Tunis	Tunis, Tunisia Hammamet, Tunisia	1050031300	5	7,103
Kairouan	Kairouan, Tunisia Kasserine, Tunisia	1050031570	5	15,262
Sfax	Sfax, Tunisia Sousse, Tunisia	1050031570	5	21,685
Zarzis	Zarzis, Tunisia Medinine, Tunisia	1050031860	5	7,405
Tripoli	Tripoli, Libya Misrata, Libya	1050032180	5	17,628
Benghazi	Benghazi, Libya Marsa Matruh, Egypt	1050032680	5	85,853

**Table 2.** Description of the studied basins. \*The basin name in this study may include several hydrologic basins and it was obtained from the main river or city.

conservation measures. Regular updates are planned to maintain data accuracy, ensuring the dataset's reliability and relevance over time.

The utility of our dataset derives from its continental coverage, high resolution, and comprehensive integration of specific regional environmental factors. Unlike broader global datasets, ours provides targeted insights into the North African context, filling a critical gap in the literature. This specificity not only enhances the dataset's relevance for local soil conservation efforts but also contributes to the global understanding of soil erosion dynamics for arid and semi-arid areas. By providing detailed soil erosion susceptibility maps and raster data for the hydrological basins of North Africa, our work aligns with global trends while offering unique, region-specific insights. This balance between regional focus and global relevance underscores the significance of our contribution to the field of soil erosion assessment.

The regional soil loss map (Fig. 3) reveals that the Sahara Desert and Egypt experience very low soil loss rates, comprising 61% of the area, while low rates, ~14%, are found around the Atlas Belt and the Libyan coast. In contrast, high soil loss rates of ~22% are observed in the Atlas Mountains range and the steep Mediterranean coastal mountains between Morocco and Tunisia, particularly in the Rif and Atlas regions. The Nile banks and Delta, along with other productive areas, also experience higher soil loss rates. This poses significant risks to vegetative productivity, especially in these climatically sensitive regions, making environmental stress from land degradation more hazardous<sup>10</sup>. Prolonged intra-annual droughts (Heggy *et al.*<sup>19</sup>) exacerbate susceptibility to soil degradation, which is amplified by intense localized rainstorms, leading to severe turbiditic floods. In upstream mountainous areas, this cumulative effect results in poor soil quality and reduced vegetation productivity<sup>45</sup>.

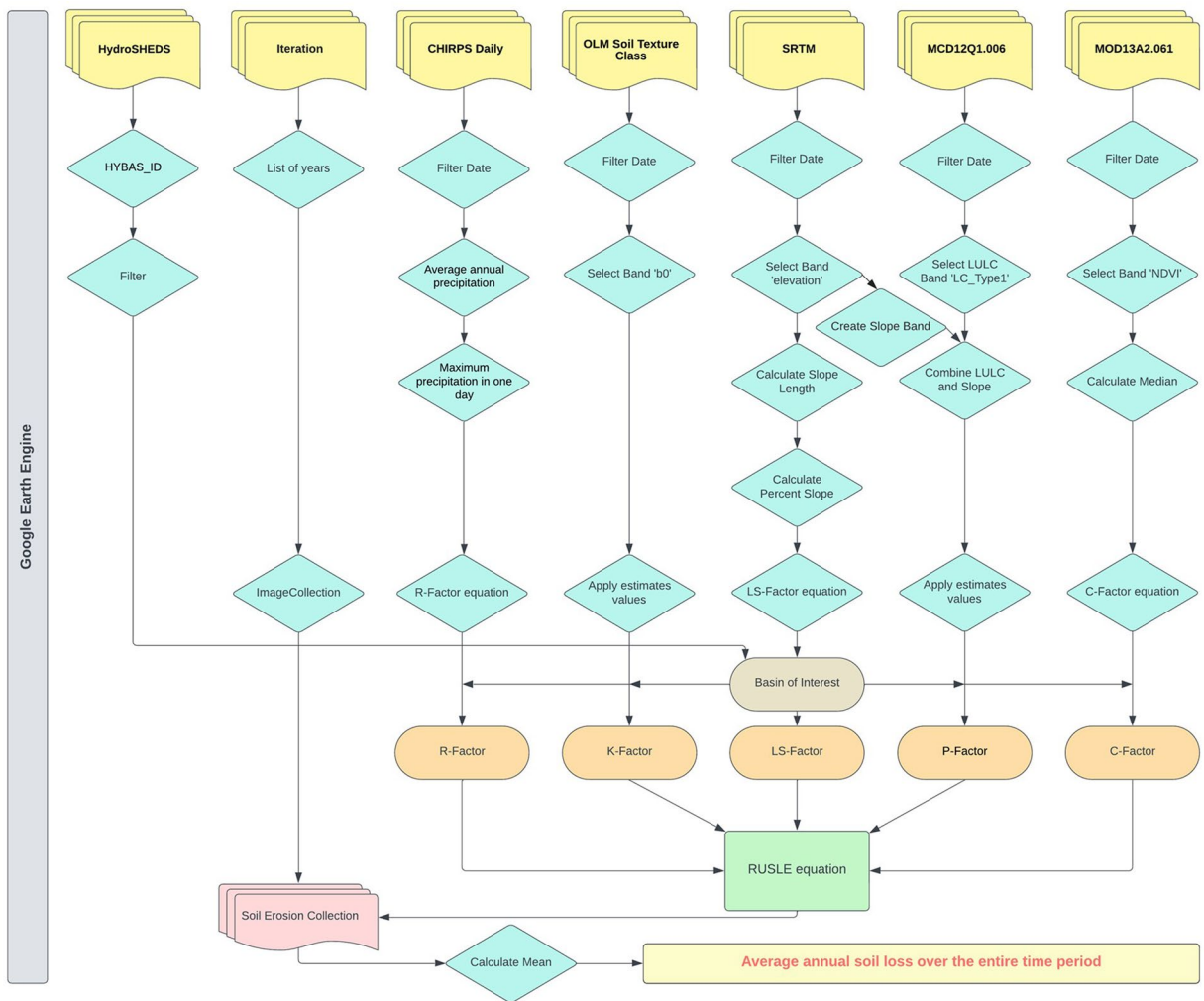


**Fig. 2** Flow chart for the generation of the SESMAR data products.

The dataset is provided in a compressed format to characterize soil loss susceptibility, categorizing each map and raster into six distinct classes, as exemplified in Fig. 3. The classification is based on the estimated annual soil loss rates per hectare<sup>46</sup>, with associated values as follows:

- 0: No Data. This category designates areas where soil loss susceptibility information is unavailable, serving as a placeholder for missing or inaccessible data.
- 1: Very Low (<5 t/ha/year). Raster cells in this class represent areas with very low susceptibility to soil loss, indicating an annual rate of less than 5 tons per hectare.
- 2: Low (5 to 15 t/ha/year). This class characterizes areas with low susceptibility, where the annual soil loss rate falls within the range of 5 to 15 tons per hectare.
- 3: Medium (15 to 50 t/ha/year). Raster cells categorized as medium susceptibility denote moderate levels of soil loss, with an annual rate ranging from 15 to 50 tons per hectare.
- 4: High (50 to 80 t/ha/year). This class identifies areas with high susceptibility to soil loss, where the annual rate ranges from 50 to 80 tons per hectare.
- 5: Very High (>80 t/ha/year). Raster cells in this category indicate the highest susceptibility to soil loss, with an annual rate exceeding 80 tons per hectare.

Our analysis also quantifies and discusses the yearly variation of soil erosion over time (Fig. 4), examining its relationship with variations in input drivers such as precipitation and land cover. The cumulative anomaly of soil loss from 2001 to 2023 reveals significant insights into erosion patterns across North Africa. In Morocco, notable positive anomalies are observed in the Northern basins and Atlantic areas, indicating increased erosion rates. Similar patterns are found in the region between Algiers and Annaba in Mediterranean Algeria, as well as in coastal areas of Tunisia and Libya, including Tunis, Kairouan, Benghazi, and Derna.

A temporal examination highlights a consistent upward trend in soil loss. The proportion of areas at medium to high risk of soil erosion has increased from 7% in 2002 to approximately 15% in recent years. These areas are

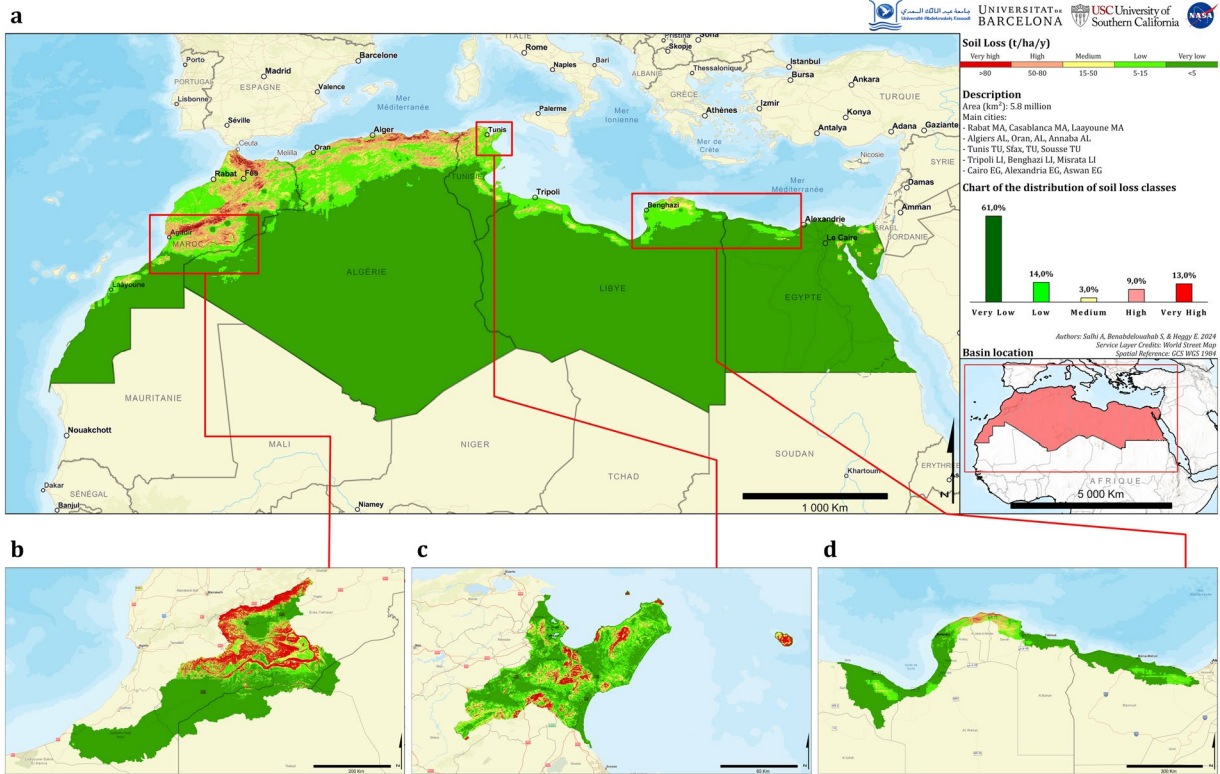


**Fig. 3** Map of the estimated average long-term (2001–2023) annual soil erosion risk in (a) North Africa. The figure includes three sample maps representing (b) the basins of Draa (Morocco), (c) Tunis (Tunisia), and (d) Coastal Mediterranean basins (Libya and Egypt). These sample maps are selected from a set of 22 available basin maps and provide detailed visualizations of the soil erosion risk within these specific regions.

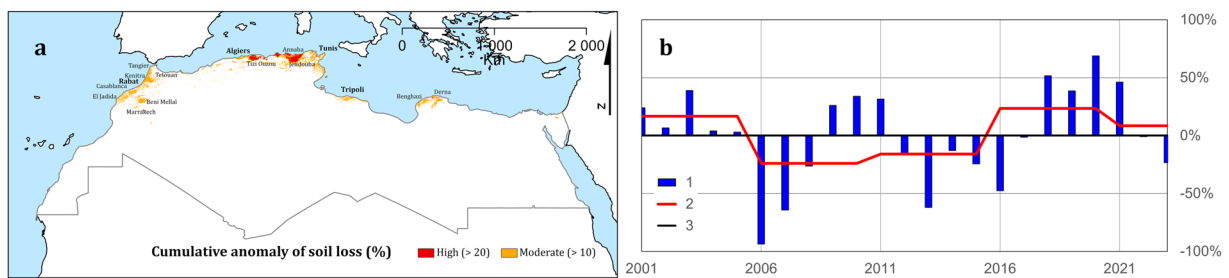


**Fig. 4** Analysis of long-term (2001–2023) soil loss in North Africa (excluding the Sahara). (a) The cumulative anomaly of soil loss with a focus on areas of high and moderate anomalies. (b) The annual soil loss anomaly chart: (1) the anomaly curve, (2) the moving 5-year average of anomalies, and (3) the average of anomalies.

often urban and located in critical zones, such as watershed outlets, which are particularly prone to flash floods<sup>47</sup>. This has resulted in an increase in the population highly vulnerable to these hazards from around 22,000 in 2002 to about 29,000 currently<sup>21</sup>. The intensification of semi-informal urban settings, along with increased rain aggressiveness and storminess, are primary drivers of this trend<sup>48,49</sup>.

Moreover, soil degradation impacts both upstream and downstream areas of watersheds. Upstream, there is a noticeable loss of fertility, degradation of water reservoir storage capacities, and impairment of critical infrastructures. Downstream, particularly in conjunction with flash floods, there is an escalating risk to human assets. According to prevailing hydroclimatic forecasts, this trend is expected to intensify, making hundreds of settlements downstream more susceptible to higher impacts<sup>50,51</sup>.

### Technical Validation

To validate the robustness of our dataset, a thorough assessment was conducted by juxtaposing our outcomes against those derived from published articles employing a comparable methodology for soil erosion estimation in North Africa. Unfortunately, a pixel-based correlation wasn't feasible due to the unavailability of granular data from these articles. Consequently, our comparison focused on the average annual soil loss (measured in t/ha/y)

Basin information		HydroBASINS <sup>38</sup>		Reported paper		Soil erosion (t/ha/y)			Soil erosion class <sup>46</sup>		
Name	Country	Watershed code	Watershed area (km <sup>2</sup> )	Reference	Watershed area (km <sup>2</sup> )	Referenced	ESDAC based Model	Modeled	Reference	ESDAC based Model	Modeled
Soummam	Algeria	1060030840	9,125	<a href="#">57</a>	9,108	6.8	11.5	8.5	Low	Low	Low
Oued Arab	Algeria	1100091790	348	<a href="#">58</a>	567	11.9	14.2	12.9	Low	Low	Low
Djelfa (Saharan Atlas)	Algeria	1060043340	4,610	<a href="#">59</a>	3,828	2.3	0.3	0.1	Very Low	Very Low	Very Low
Tlemcen	Algeria	1060030310	7811	<a href="#">60</a>	Not indicated	1.5 to 6.8	3.5	2.7	Very Low	Very Low	Very Low
Maleh	Algeria	1080087230	886	<a href="#">61</a>	933	2.9	1.4	4.8	Very Low	Very Low	Very Low
Naghamish	Egypt	1100033970	112	<a href="#">62</a>	90	1.4	1.7	1.9	Very Low	Very Low	Very Low
Northwestern coast	Egypt	1060033680	7,123	<a href="#">63</a>	9,182	2.1	0.8	<4.0	Very Low	Very Low	Very Low
Ras El-Hekma (Matrouh)	Egypt	1120034020	372	<a href="#">64</a>	Not indicated	6.7	1.4	7.5	Low	Very Low	Low
Derna	Lybia	1090033270	574	<a href="#">65</a>	570	Not referenced	3.5	5.2	Not studied	Very Low	Low
Nekor	Morocco	1070030070	911	<a href="#">27</a>	916	37.8	21.2	23.4	Medium	Medium	Medium
Bouregreg	Morocco	1070029670	9,894	<a href="#">66</a>	10,000	20.0	26.0	16.6	Medium	Medium	Medium
Upper Sebou	Morocco	1060099860	7392	<a href="#">67</a>	5,495	6.5	14.7	14.4	Low	Low	Low
Melloussa	Morocco	1100029820	123	<a href="#">20</a>	121	11.6	27.8	26.5	Low	Medium	Medium
Tangier	Morocco	1090029800	269	<a href="#">29</a>	254	24.2	18.1	21.6	Medium	Medium	Medium
Ghis	Morocco	1080030050	831	<a href="#">28</a>	845	30.1	48.3	39.0	Medium	Medium	Medium
Tensift	Morocco	1060029350	20,344	<a href="#">68</a>	20,450	44.0	18.2	25.0	Medium	Medium	Medium
Ikkour	Morocco	1100115610	198	<a href="#">69</a>	55	0.7	17.3	11.4	Very Low	Medium	Low
N'fis	Morocco	1070129680	2,928	<a href="#">70</a>	1,704	25.8	37.4	52.6	Medium	Medium	High
Koutine	Tunisia	1100031990	396	<a href="#">71</a>	279	1.0	0.6	0.2	Very Low	Very Low	Very Low
Chiba	Tunisia	1100031520	206	<a href="#">72</a>	204	11.8	1.8	3.6	Low	Very Low	Very Low

**Table 3.** Comparative analysis of the modeled soil erosion in North African watersheds with data from published articles.

and involved a meticulous visual inspection of the generated maps. In our scrutiny, 20 watersheds from diverse North African countries and characteristics were selected, ensuring a comprehensive representation of climatic, topographic, and land use conditions. Leveraging the extensive HydroBASINS database, which furnishes a global repository of drainage basins across various scales, we meticulously curated watershed information (Table 3).

This in-depth analysis suggests a resemblance in terms of average annual soil loss values, coupled with a concordance with soil erosion classes as defined in previous studies<sup>46</sup>. The visual scrutiny at the watershed level underscored an alignment in the distribution of different soil erosion classes, attesting to a high degree of concordance between our model and the referenced studies.

While some minor discrepancies emerged in the average annual soil loss values, these can be attributed to variations in datasets, spatial and temporal scales, and pixel resolutions used by different teams. However, our dataset demonstrates strong accuracy across a diverse range of watersheds, each with unique dimensions, morphologies, and local conditions. These minor differences remain within the same erosion classes, underscoring the robustness of our findings for strategic decision-making. Notably, our dataset demonstrates strong accuracy across all watersheds (22), with only two exceptions. We also recognize the potential for further refinement in future studies through methodological enhancements and using higher-quality data to improve fine-scale (local) results.

To further validate the soil erosion susceptibility model, we incorporate global lower-resolution data sources, specifically using the ESDAC-based K-factor (1 km resolution)<sup>4,52</sup> and comparing results to the GloREDa R-factor dataset<sup>53,54</sup>. This adjustment aims at evaluating the consistency and accuracy of the SESMAR model (500 m resolution) against a different modeling approach and data resolution. The ESDAC-based model was adapted to match the spatial extent and hydrological basins used in the SESMAR approach, enabling side-by-side comparison of the predicted soil erosion susceptibility across different watersheds in North Africa.

The two models are compared according to pixel-based and quantitative inspections. Figure 5 illustrates the differences in soil erosion susceptibility mapping derived from the SESMAR model (panels a, c, e, g) and the ESDAC-based model (panels b, d, f, h). Notably, the ESDAC model's lower spatial resolution resulted in a broader classification of areas as 'high' or 'very high' susceptibility, particularly in regions with more complex topography, while the SESMAR model showed more detailed patterns of erosion risk. Additionally, data gaps are observed in the ESDAC-based maps, underscoring the limitations of using lower-resolution datasets.

The comparative analysis of the SESMAR and ESDAC-based models reveals a distinct spatial distribution of erosion risk classes across various watersheds (Table 3). This highlights the models' respective abilities to capture local variations in erosion susceptibility. Indeed, both models showed consistency in identifying areas with very low and low erosion risk across many watersheds. For instance, in the Djelfa basin (Saharan Atlas, Algeria), both models classified the watershed as "Very Low" erosion, with SESMAR reflecting finer resolution variations

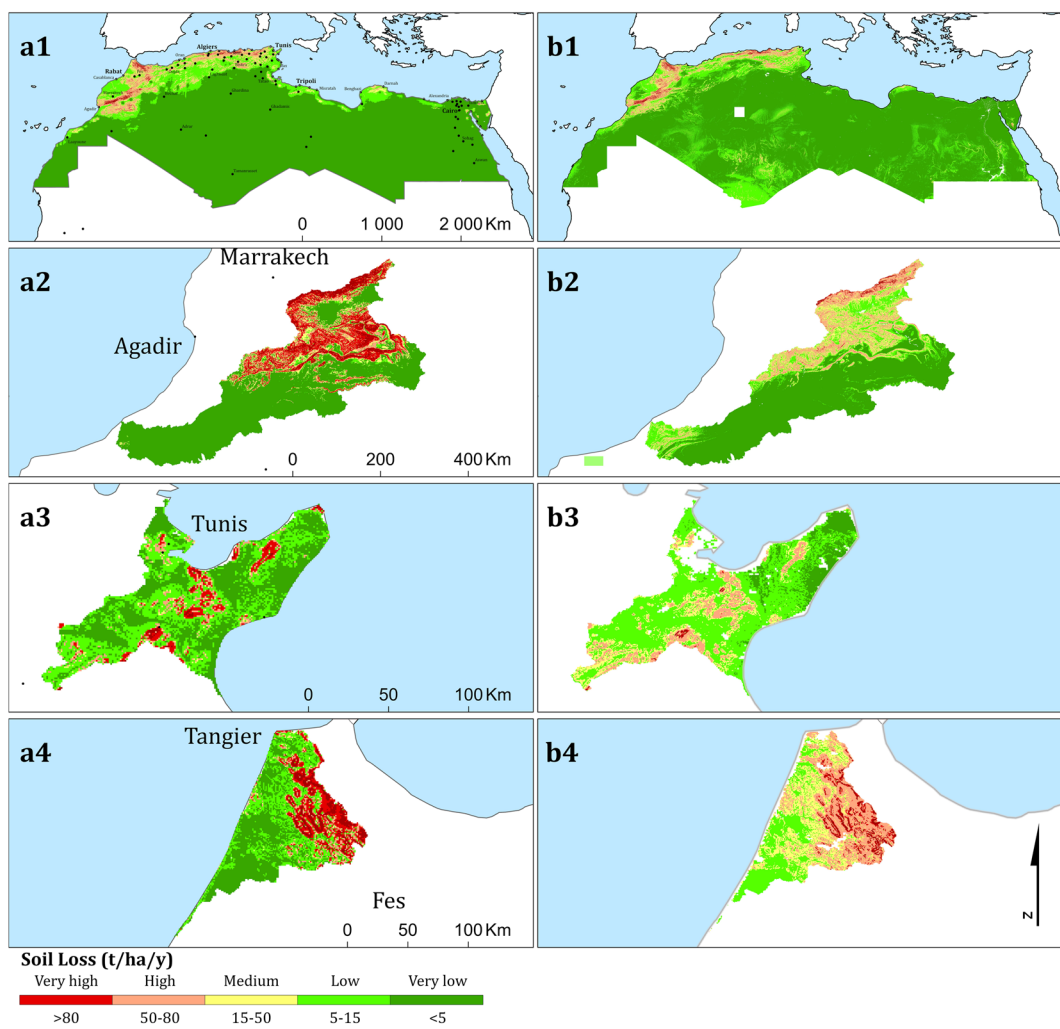


**Fig. 5** Comparison of soil erosion susceptibility maps using different data sources and modeling approaches. Panels (a1, a2, a3, a4) present results from the first approach (SESMAR), while panels (b1, b2, b3, b4) show outcomes based on the second approach (ESDAC-based model).

despite similar overall class assignments. Similarly, in the Noghamish basin in Egypt, both models classified erosion susceptibility as “Very Low,” indicating minimal discrepancies in areas with inherently low erosion risks.

However, the models diverged considerably regarding watersheds exhibiting medium or higher erosion risks. In the Melloussa watershed (Morocco), for example, the SESMAR model classified the area as “Medium” susceptibility, while the ESDAC-based model categorized it as “Low” because of SESMAR’s capacity to detect more localized erosion risks, likely due to its higher resolution (500 m vs. 1 km). A similar pattern was observed in the N’fis watershed, where SESMAR assigned a “High” erosion class compared to the “Medium” classification by ESDAC, underscoring SESMAR’s sensitivity to high-risk erosion zones. In watersheds with a range of erosion risks, SESMAR’s classification demonstrated a more detailed identification of areas transitioning from low to medium erosion classes. For example, in the Nekor and Bouregreg basins (Morocco), the SESMAR model classified these areas as “Medium” erosion, aligning more closely with published studies than the ESDAC model, which tended to generalize larger portions as “Medium” without capturing finer spatial distinctions. The SESMAR model’s higher resolution allowed for better mapping of medium-risk zones, reflecting the natural heterogeneity of erosion susceptibility across the watershed. In regions with frequent spatial variations, such as the Ghis watershed (Morocco), the SESMAR model’s spatial classification differed from ESDAC’s broader categorization of similar susceptibility, suggesting SESMAR’s better performance in pinpointing high-risk zones, which is crucial for prioritizing erosion control measures.

The differences in soil erosion class predictions between the SESMAR and ESDAC models have significant implications for erosion management strategies. The SESMAR model’s more detailed classification of medium to high erosion-risk areas allows for more precise targeting of erosion control measures, particularly in high-risk watersheds. The model’s capacity to detect variations within these classes can guide the allocation of resources to the most vulnerable zones. Also, the comparison underscores the limitations of lower-resolution data in capturing detailed spatial patterns of erosion susceptibility. The ESDAC model’s broader classification of larger

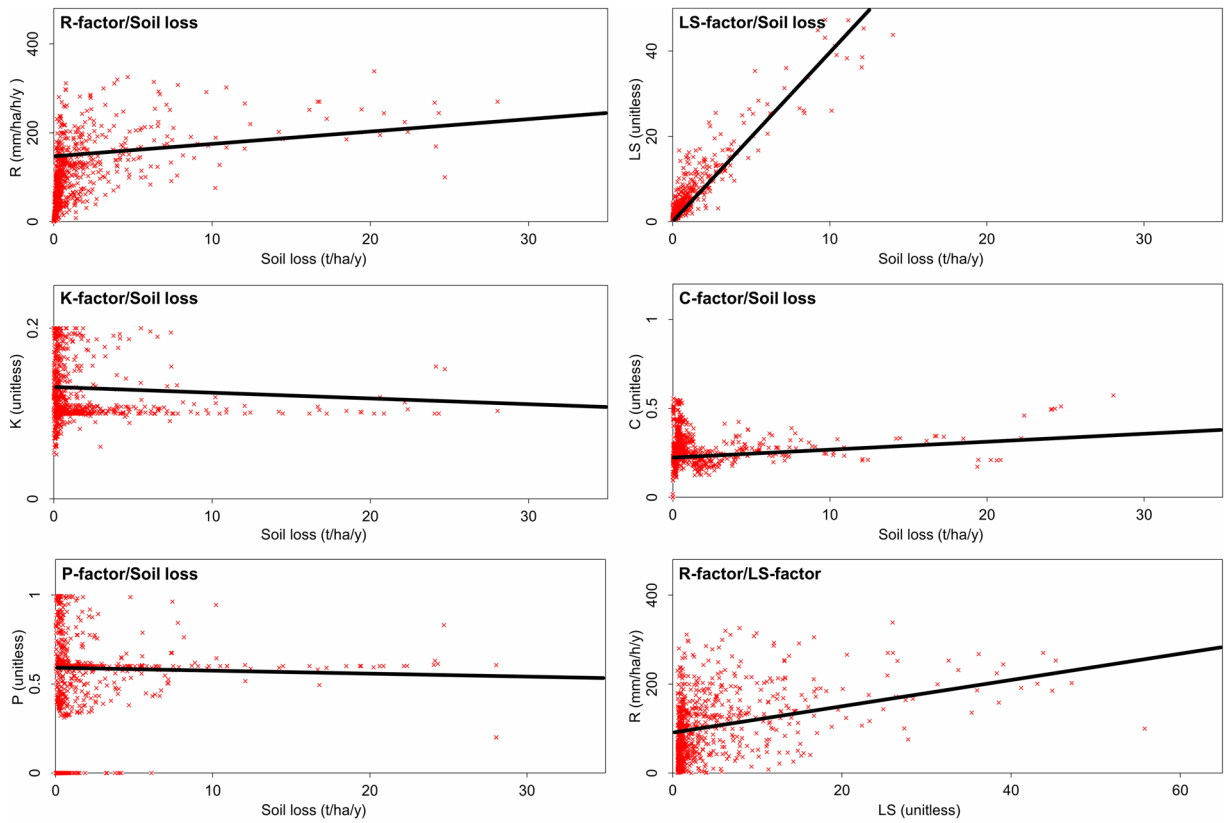


**Fig. 6** Pixel-based correlation between estimated soil loss and soil erosion factors.

areas into single erosion classes may overlook important localized differences, which could lead to inefficient mitigation planning.

Consequently, while both models can provide useful information for regional soil erosion assessment, the SESMAR model's higher resolution and finer classification of erosion risks make it better suited for applications requiring detailed erosion management strategies, namely in North Africa.

Additionally, a pixel-based analysis was employed to assess the spatial variations of erosion factors ( $R$ ,  $K$ ,  $LS$ ,  $P$ , and  $C$ ) and their correlation with soil loss rates (Fig. 6). Firstly, a positive linear correlation appears between soil loss and the  $R$ -factor (rainfall aggressivity), accompanied by a positive linear correlation with the  $LS$ -factor (length-slope). Both correlations imply that as the  $R$ -factor and  $LS$ -factor increase, soil loss intensifies, underscoring the direct impact of slope characteristics and rainfall intensity on erosion rates. Significantly, a positive linear correlation emerges between the  $LS$ -factor and the  $R$ -factor, indicating that the combined effect of length, slope, and rainfall intensity contribute to heightened soil loss. Conversely, a negative linear correlation is observed between soil loss and the  $K$ -factor (soil erodibility), emphasizing the influence of soil characteristics, particularly granulometry, on erosion dynamics.

For  $C$ -factor (cover management) and  $P$ -factor (support practices), weak positive linear correlations and negative correlations, respectively, hint at potential relationships with soil loss, although their significance is less pronounced compared to other factors. These findings suggest that as the  $C$ -factor increases (or  $P$ -factor decreases), there might be a slight uptick in soil loss, but the relationship is not as robust as observed with the  $R$ -factor or  $LS$ -factor. It is crucial to note that despite these weak linear correlations, the potential for non-linear relationships in the  $C$ -factor,  $P$ -factor, and soil loss dynamics exists. While these correlations contribute to understanding the factors influencing soil loss processes, the complex relationships in the  $C$ -factor and  $P$ -factor do not neatly align with simple linear correlations, emphasizing the necessity for further investigations.

Our pixel-based extensive analysis furnishes valuable insights into broader patterns and trends shaping soil loss dynamics in North Africa. However, acknowledging resolution limitations is essential, as they may lead to the underrepresentation of small-scale cover management and support practices. To address this limitation, local case studies are encouraged to explore the complex dynamics of these factors at a finer scale.

The interplay of adverse climatic and environmental conditions, marked by prolonged droughts succeeded by intense storms, have exacerbated soil loss, contributing to a decline in vegetation cover<sup>55,56</sup>. Conversely, extended wet periods have facilitated the med-term progression of vegetation productivity, diminishing its correlation with soil loss. Another contributing factor to the weak correlation is that North Africa exhibits significant vegetation cover only in a restricted northern coastal area where high soil loss values were observed, while elsewhere, vegetation productivity is very low or soil loss rates are low, rendering its correlation inconclusive. Notably, areas north of the Atlas Belt stand out as particularly vulnerable to the risks associated with soil loss.

## Code availability

The code used in this study is freely available at <https://doi.org/10.5281/zenodo.12701613>, facilitating reproducibility and transparency in the analysis conducted.

Received: 29 April 2024; Accepted: 3 January 2025;

Published online: 14 January 2025

## References

- Normand, J. C. L. & Heggy, E. Assessing flash flood erosion following storm Daniel in Libya. *Nat Commun* **15**, 6493, <https://doi.org/10.1038/s41467-024-49699-8> (2024).
- Piemontese, L., Fetzer, I., Rockström, J. & Jaramillo, F. Future hydroclimatic impacts on Africa: beyond the Paris agreement. *Earth's Future* **7**, 748–761 (2019).
- Salhi, A., Benabdoulaahab, S. & Martin-Vide, J. Statistical analysis of long-term precipitation in the Maghreb reveals significant changes in timing and intensity. *Theoretical and Applied Climatology* <https://doi.org/10.1007/s00704-022-04236-9> (2022).
- Borrelli, P. *et al.* An assessment of the global impact of 21st century land use change on soil erosion. *Nature Communications* **8**, 2013, <https://doi.org/10.1038/s41467-017-02142-7> (2017).
- Wuepper, D., Borrelli, P. & Finger, R. Countries and the global rate of soil erosion. *Nature sustainability* **3**, 51–55 (2020).
- Borrelli, P. *et al.* A step towards a holistic assessment of soil degradation in Europe: Coupling on-site erosion with sediment transfer and carbon fluxes. *Environmental Research* **161**, 291–298, <https://doi.org/10.1016/j.envres.2017.11.009> (2018).
- Clement, V. *et al.* (World Bank, 2021).
- García-Ruiz, J. M., Beguería, S., Lana-Renault, N., Nadal-Romero, E. & Cerdà, A. Ongoing and emerging questions in water erosion studies. *Land Degradation & Development* **28**, 5–21 (2017).
- Benassi, F., Carella, M. & Heins, F. J. I. G. Migration in the Mediterranean region: A response to crises and an emergency in its own right. 15–36 (2022).
- Salhi, A., Vila Subirós, J. & Insalaco, E. Spatial patterns of environmental degradation and demographic changes in the Mediterranean fringes. *Geocarto International*, 1–17, <https://doi.org/10.1080/10106049.2022.2090619> (2022).
- Wischmeier, W. H. & Smith, D. D. *Predicting rainfall erosion losses: a guide to conservation planning*. (Department of Agriculture, Science and Education Administration, 1978).
- Persits, F. M. *et al.* Maps showing geology, oil and gas fields and geological provinces of Africa. Report No. 97-470A, (Reston, VA, 1997).
- Bouabdellah, M. & Slack, J. F. In *Mineral Deposits of North Africa* (eds Mohammed Bouabdellah & John F. Slack) 3–81 (Springer International Publishing, 2016).
- Avigad, D. *et al.* Mass-production of Cambro-Ordovician quartz-rich sandstone as a consequence of chemical weathering of Pan-African terranes: Environmental implications. *Earth and Planetary Science Letters* **240**, 818–826, <https://doi.org/10.1016/j.epsl.2005.09.021> (2005).
- Hoepffner, C., Houari, M. R. & Bouabdelli, M. Tectonics of the North African Variscides (Morocco, western Algeria): an outline. *Comptes Rendus Geoscience* **338**, 25–40, <https://doi.org/10.1016/j.crte.2005.11.003> (2006).
- Tawadros, E. *Geology of North Africa*. (CRC Press, 2011).
- Salhi, A. & Benabdoulaahab, S. The downstream impact of the first and second filling of the Grand Ethiopian Renaissance Dam. *Sustainable Water Resources Management* **9** (2022).
- Heggy, E., Sharkawy, Z. & Abotalib, A. Z. Egypt's water budget deficit and suggested mitigation policies for the Grand Ethiopian Renaissance Dam filling scenarios. *Environmental Research Letters* **16**, 074022 (2021).
- Heggy, E., Ramah, M. & Abotalib, A. Z. Examining the Accuracy of Using a Single Short-Term Historical Flow Period to Assess the Nile's Downstream Water Deficit from GERD Filling: A Technical Note. *Earth Systems and Environment* **7**, 723–732 (2023).
- Salhi, A. *et al.* Impact of massive development projects on ecosystem services in Mediterranean rural landscapes. *Remote Sensing Applications: Society and Environment* **29**, 100880, <https://doi.org/10.1016/j.rsase.2022.100880> (2023).
- Salhi, A., Benabdoulaahab, S. & Heggy, E. Growing soil erosion risks and their role in modulating catastrophic floods in North Africa. *International Journal of Applied Earth Observation and Geoinformation* **133**, 104132, <https://doi.org/10.1016/j.jag.2024.104132> (2024).
- Sadiki, A., Bouhlassa, S., Auajjar, J., Fahel, A. & Macaire, J.-J. Utilisation d'un SIG pour l'évaluation et la cartographie des risques d'érosion par l'Équation universelle des pertes en sol dans le Rif oriental (Maroc): cas du bassin versant de l'oued Boussouab. *Bulletin de l'Institut Scientifique, Rabat, section Sciences de la Terre* **26**, 69–79 (2004).
- Okacha, A. & Salhi, A. Refining erosion assessment with NDVI-based modeling: a case study in diverse climatic zones. *Mediterranean Geoscience Reviews*, <https://doi.org/10.1007/s42990-024-00134-6> (2024).
- Nearing, M. A., Yin, S.-q., Borrelli, P. & Polyakov, V. O. Rainfall erosivity: An historical review. *Catena* **157**, 357–362 (2017).
- Yin, S., Nearing, M. A., Borrelli, P. & Xue, X. Rainfall erosivity: An overview of methodologies and applications. *Vadose Zone Journal* **16**, 1–16 (2017).
- Oliveira, P. T. S., Wendland, E. & Nearing, M. A. Rainfall erosivity in Brazil: A review. *Catena* **100**, 139–147 (2013).
- Okacha, A., Salhi, A., Arari, K., Elbadaou, K. & Lahrichi, K. Soil erosion assessment using the RUSLE model for better planning: a case study from Morocco. *Modeling Earth Systems and Environment*, <https://doi.org/10.1007/s40808-023-01731-4> (2023).
- Salhi, A. *et al.* Bridging the gap of perception is the only way to align soil protection actions. *Science of the Total Environment* **718**, 137421, <https://doi.org/10.1016/j.scitotenv.2020.137421> (2020).
- Salhi, A., El Hasnaoui, Y., Pérez Cutillas, P. & Heggy, E. Soil erosion and hydroclimatic hazards in major African port cities: the case study of Tangier. *Scientific Reports* **13**, 13158, <https://doi.org/10.1038/s41598-023-40135-3> (2023).
- Benavidez, R., Jackson, B., Maxwell, D. & Norton, K. A review of the (Revised) Universal Soil Loss Equation ((R) USLE): with a view to increasing its global applicability and improving soil loss estimates. *Hydrology and Earth System Sciences* **22**, 6059–6086 (2018).
- USDA-NRCS. *Revised Universal Soil Loss Equation, Version 2 (RUSLE2) estimates soil loss caused by rainfall and its associated overland flow*, <https://www.nrcs.usda.gov/resources/tech-tools/water-erosion-rusle2> (2024).
- FAO. *FAO guidelines for land evaluation: Revised Universal Soil Loss Equation*, <https://www.fao.org/land-water/land/land-governance/land-resources-planning-toolbox/category/details/en/c/1236444/> (2024).
- Rawat, K. S. & Singh, S. K. Appraisal of Soil Conservation Capacity Using NDVI Model-Based C Factor of RUSLE Model for a Semi Arid Ungauged Watershed: a Case Study. *Water Conservation Science and Engineering* **3**, 47–58, <https://doi.org/10.1007/s41101-018-0042-x> (2018).
- Ayalew, D. A., Deumlich, D., Šarapatka, B. & Doktor, D. Quantifying the Sensitivity of NDVI-Based C Factor Estimation and Potential Soil Erosion Prediction using Spaceborne Earth Observation Data. *Remote Sensing* **12** (2020).
- Prasannakumar, V., Vijith, H., Geetha, N. & Shiny, R. Regional scale erosion assessment of a sub-tropical highland segment in the Western Ghats of Kerala, South India. *Water resources management* **25**, 3715–3727 (2011).
- Van der Knijff, J. M. F., Jones, R. J. A. & Montanarella, L. *Soil erosion risk assessment in Italy*. (Citeseer, 1999).
- Valor, E. & Caselles, V. Mapping land surface emissivity from NDVI: Application to European, African, and South American areas. *Remote Sensing of Environment* **57**, 167–184, [https://doi.org/10.1016/0034-4257\(96\)00039-9](https://doi.org/10.1016/0034-4257(96)00039-9) (1996).

38. Lehner, B. & Grill, G. Global river hydrography and network routing: baseline data and new approaches to study the world's large river systems. *Hydrological Processes* **27**, 2171–2186 (2013).
39. Funk, C. *et al.* The climate hazards infrared precipitation with stations—a new environmental record for monitoring extremes. *Scientific data* **2**, 1–21 (2015).
40. Hengl, T. Soil texture classes (USDA system) for 6 soil depths (0, 10, 30, 60, 100 and 200 cm) at 250 m. *Zenodo, December* **24** (2018).
41. Farr, T. G. *et al.* The shuttle radar topography mission. *Reviews of geophysics* **45** (2007).
42. Didan, K. MODIS/Terra Vegetation Indices 16-Day L3 Global 250m SIN Grid V061 [Data set]. NASA EOSDIS Land Processes DAAC. (Accessed 2023-12-23 from <https://doi.org/10.5067/MODIS/MOD13Q1.061>, 2021).
43. Friedl, M. & Sulla-Menashe, D. MCD12Q1 MODIS/Terra+ aqua land cover type yearly L3 global 500m SIN grid V006. NASA EOSDIS Land Processes DAAC **10**, 200 (2019).
44. Salhi, A., Benabdellahab, S. & Heggy, E. SESMAR - Soil Erosion Susceptibility Maps And Raster dataset for the hydrological basins of North Africa. *Zenodo (Dataset) Vers. 1. Zenodo* <https://doi.org/10.5281/zenodo.1047896> (2024).
45. Panagos, P. & Katsoyiannis, A. Soil erosion modelling: The new challenges as the result of policy developments in Europe. *Journal of Environmental Research* **172**, 470–474 (2019).
46. Zachar, D. *Soil Erosion*. (Elsevier Scientific Publishing Company, 1982).
47. Derdouri, A. *et al.* Coastal satellite urbanization in the global south: Dynamics, sustainability dilemmas, and pathways for Martil, Morocco. *Cities* **149**, 104981, <https://doi.org/10.1016/j.cities.2024.104981> (2024).
48. Salhi, A., Larifi, I., Salhi, H. & Heggy, E. Flooding in semi-uniform urban areas in North Africa: Environmental and psychosocial drivers. *Science of The Total Environment*, 172486, <https://doi.org/10.1016/j.scitotenv.2024.172486> (2024).
49. Tramblay, Y. *et al.* Regional flood frequency analysis in North Africa. *Journal of Hydrology* **630**, 130678 (2024).
50. Waha, K. *et al.* Climate change impacts in the Middle East and Northern Africa (MENA) region and their implications for vulnerable population groups. *Regional Environmental Change* **17**, 1623–1638 (2017).
51. IPCC. Climate change 2023: synthesis report. Contribution of working groups I, II and III to the sixth assessment report of the intergovernmental panel on climate change. Report No. 929169164X, 184 (IPCC, Geneva, Switzerland, 2023).
52. Gupta, S., Borrelli, P., Panagos, P. & Alewell, C. An advanced global soil erodibility (K) assessment including the effects of saturated hydraulic conductivity. *Science of The Total Environment* **908**, 168249, <https://doi.org/10.1016/j.scitotenv.2023.168249> (2024).
53. Panagos, P. *et al.* Global rainfall erosivity database (GloREDa) and monthly R-factor data at 1 km spatial resolution. *Data in Brief* **50**, 109482, <https://doi.org/10.1016/j.dib.2023.109482> (2023).
54. Panagos, P. *et al.* Global rainfall erosivity assessment based on high-temporal resolution rainfall records. *Scientific Reports* **7**, 4175, <https://doi.org/10.1038/s41598-017-04282-8> (2017).
55. Perez Cutillas, P. & Salhi, A. Long-Term Hydroclimatic Projections and Climate Change Scenarios at a National Scale in Morocco. Available at SSRN 4821787, <https://doi.org/10.2139/ssrn.4821787> (2024).
56. Okacha, A. *et al.* High-Resolution Precipitation Mapping for Morocco: Integrating Orographic and Geographic Influences. *European Modern Studies Journal* **8**, 531–549, [https://doi.org/10.59573/emsj.8\(2\).2024.45](https://doi.org/10.59573/emsj.8(2).2024.45) (2024).
57. Sahli, Y. *et al.* Mapping surface water erosion potential in the Soummam watershed in Northeast Algeria with RUSLE model. *Journal of Mountain Science* **16**, 1606–1615 (2019).
58. Koussa, M. & Bouziane, M.-T. Estimation des paramètres de l'érosion hydrique par Approche SIG/USLE: cas du bassin versant de l'Oued Arab (région de Khenchela, Nord-Est de l'Algérie)[Estimation of water erosion parameters by GIS/USLE approach: Case of the Oued Arab watershed (Khenchela region, North-East Algeria)]. *Agriculture and Forestry Journal* **3**, 36–45 (2019).
59. Boussadia-Omari, L. *et al.* Contribution of phytoclimatic data to spatialize soil erosion: Application of the RUSLE model in the Algerian atlas. *International Soil and Water Conservation Research* **9**, 502–519, <https://doi.org/10.1016/j.iswcr.2021.05.004> (2021).
60. Morsli, B., Habi, M. & Meddi, M. Dynamique de l'érosion en zone méditerranéenne algérienne: facteurs explicatifs de variation du ruissellement et de l'érosion sous différentes occupations du sol. *Revue des sciences de l'eau* **26**, 89–105 (2013).
61. Benselama, O., Mazour, M., Hasbaïa, M., Djoukbal, O. & Mokhtari, S. Prediction of water erosion sensitive areas in Mediterranean watershed, a case study of Wadi El Maleh in north-west of Algeria. *Environmental Monitoring and Assessment* **190**, 735, <https://doi.org/10.1007/s10661-018-7117-1> (2018).
62. Azab, Y. F. A. *et al.* Soil erosion assessment in arid region: A case study in Wadi Naghamish, Northwest Coast, Egypt. *The Egyptian Journal of Remote Sensing and Space Science* **24**, 1111–1118, <https://doi.org/10.1016/j.ejrs.2021.11.008> (2021).
63. Mohamed, E. S., Schütt, B. & Belal, A. Assessment of environmental hazards in the north western coast -Egypt using RS and GIS. *The Egyptian Journal of Remote Sensing and Space Science* **16**, 219–229, <https://doi.org/10.1016/j.ejrs.2013.11.003> (2013).
64. Kassab, M. F., Hassanin, W. F., Mostafa, A. M. & Benmansour, M. Assessment of erosion rate in a rainfed agricultural area on the Northwestern coast of Egypt using  $^{137}\text{Cs}$  measurements. *Journal of Environmental Radioactivity* **246**, 106851, <https://doi.org/10.1016/j.jenrad.2022.106851> (2022).
65. Ashour, M. A., Aly, T. E. & Abuleyoun, H. M. Transboundary water resources “A comparative study”: The lessons learnt to help solve the Nile basin water conflict. *Limnological Review* **19**, 3–14 (2019).
66. Hara, F., Achab, M., Emran, A. & Mahe, G. Study of soil erosion risks using RUSLE Model and remote sensing: case of the Bouregreg watershed (Morocco). *Proceedings of the International Association of Hydrological Sciences* **383**, 159–162 (2020).
67. Boufala, M. H. *et al.* Hydrological modeling of water and soil resources in the basin upstream of the Allal El Fassi dam (Upper Sebou watershed, Morocco). *Modeling Earth Systems and Environment* **5**, 1163–1177, <https://doi.org/10.1007/s40808-019-00621-y> (2019).
68. Meliho, M., Khattabi, A. & Mhammdi, N. Spatial assessment of soil erosion risk by integrating remote sensing and GIS techniques: a case of Tensift watershed in Morocco. *Environmental Earth Sciences* **79**, 207, <https://doi.org/10.1007/s12665-020-08955-y> (2020).
69. El Jazouli, A. *et al.* Soil erosion modeled with USLE, GIS, and remote sensing: a case study of Ikkour watershed in Middle Atlas (Morocco). *Geoscience Letters* **4**, 25, <https://doi.org/10.1186/s40562-017-0091-6> (2017).
70. Markhi, A., Laftouhi, N., Grusson, Y. & Soulaimani, A. Assessment of potential soil erosion and sediment yield in the semi-arid N'fis basin (High Atlas, Morocco) using the SWAT model. *Acta Geophysica* **67**, 263–272, <https://doi.org/10.1007/s11600-019-00251-z> (2019).
71. Ben Zaied, M., Jomaa, S. & Ouessar, M. Soil Erosion Estimates in Arid Region: A Case Study of the Koutine Catchment, Southeastern Tunisia. *Applied Sciences* **11** (2021).
72. Mosbahi, M. & Benabdallah, S. Land use/land cover dynamics impact on soil erosion using GIS and Remote Sensing: a case study of Chiba basin, Northeastern Tunisia. *Arabian Journal of Geosciences* **15**, 735, <https://doi.org/10.1007/s12517-022-09978-4> (2022).

## Acknowledgements

This research was supported by internal funds from the University of Abdelmalek Essaadi. Part of this work was supported by the National Aeronautics and Space Administration under a subcontract to the California Institute of Technology and the University of Southern California and in part by the Arid and Water Research Center, University of Southern California, under the Zumberge Research and Innovation Fund. This research received support from the National Centre for Scientific and Technical Research (CNRST, Morocco) [contracts number PPR/11/2015 and IK/2018/48].

### Author contributions

All the authors of this paper have contributed substantially to the work reported. A.S. and E.H conceived the research, the code, and the modeling. S.B. led the analysis and mapping. A.S. and E.H. wrote the paper. All authors have read and agreed to the published version of the paper.

### Competing interests

The authors declare that they have no competing financial interests or personal relationships that could have appeared to influence the work reported in this paper.

### Additional information

**Correspondence** and requests for materials should be addressed to A.S.

**Reprints and permissions information** is available at [www.nature.com/reprints](http://www.nature.com/reprints).

**Publisher's note** Springer Nature remains neutral with regard to jurisdictional claims in published maps and institutional affiliations.



**Open Access** This article is licensed under a Creative Commons Attribution-NonCommercial-NoDerivatives 4.0 International License, which permits any non-commercial use, sharing, distribution and reproduction in any medium or format, as long as you give appropriate credit to the original author(s) and the source, provide a link to the Creative Commons licence, and indicate if you modified the licensed material. You do not have permission under this licence to share adapted material derived from this article or parts of it. The images or other third party material in this article are included in the article's Creative Commons licence, unless indicated otherwise in a credit line to the material. If material is not included in the article's Creative Commons licence and your intended use is not permitted by statutory regulation or exceeds the permitted use, you will need to obtain permission directly from the copyright holder. To view a copy of this licence, visit <http://creativecommons.org/licenses/by-nc-nd/4.0/>.

© The Author(s) 2025